

## X-ray transmission technique to study carbon dioxide in the critical region

Scott A. Nemmers and Harold D. Bale

*Physics Department, Box 7129, University of North Dakota, Grand Forks, North Dakota 58202-7129*

(Received 10 August 1994)

An x-ray transmission technique, which utilized a diverging x-ray beam and a position sensitive detector, was used to determine density profiles for carbon dioxide in the critical region. This x-ray technique, which does not depend upon the determination of the dielectric constant, offered a means by which previous values of the critical exponent for the order parameter, the law of rectilinear diameter, and the isothermal compressibility for carbon dioxide could be verified. Results from this procedure were compared with the best available data obtained by optical methods. Results from the analysis obtained via this technique were in close agreement with values for the critical exponent and the scaling law for coexisting phases obtained by an optical method. However, analysis of the coexistence curve diameter showed a marked divergence from rectilinear behavior in the reduced temperature region  $t < 10^{-4}$ , which was not indicated by density measurements obtained by optical techniques. Due to the statistical error associated with the density profile data, it was impossible to confirm the predicted discontinuity of the isothermal compressibility across the coexistence curve.

PACS number(s): 64.70.Fx, 07.85.-m

### I. INTRODUCTION

During the past 25 years, nearly all of the more extensive studies of fluid densities in the critical region have utilized either optical or capacitive techniques. These density determinations are based either on the measurement of the index of refraction  $n$  or the static dielectric constant  $\epsilon$ . Both techniques assume that there is a regular relationship between  $\epsilon$  and  $n$  and changes in density based upon the Clausius-Mossotti or Lorentz-Lorenz equations. The primary reliance on these methods is somewhat disquieting in that there has long been concern that the dielectric constant, and hence the index of refraction, might be anomalous at the critical point [1]. Experimental evidence suggests that the extent of the anomaly is larger for polar fluids than for nonpolar fluids [2]. Although the best estimates indicate that no special corrections are necessary in the use of either the Clausius-Mossotti equation or the Lorentz-Lorenz equation for systems with reduced temperatures  $t = (T - T_c)/T_c$  greater than  $10^{-4}$  [3], nevertheless there remains a fundamental concern when these equations serve as a basis for studying small effects. One of these effects is the anomaly in the rectilinear diameter, which only becomes evident at reduced temperatures less than  $10^{-3}$ .

This paper presents an alternative method by which the density profile of a fluid in the critical region may be more directly determined using x-ray transmission measurements. The technique, which utilized a diverging x-ray beam and a one-dimensional position sensitive detector, was used to study carbon dioxide in the critical region.

### II. X-RAY ABSORPTION

The attenuation of a monochromatic x-ray beam with incident intensity  $I_0$  on passing through a layer of materi-

al of thickness  $x$  and density  $\rho$  is governed by the well-known equation

$$I = I_0 \exp(-\mu_m \rho x), \quad (1)$$

where  $I$  is the intensity of the emergent beam and  $\mu_m$  is the mass absorption coefficient for the material. It is found that  $\mu_m$  for a given substance is approximately additive with respect to the mass absorption coefficients of which it is composed [4], namely,

$$\mu_{m,\text{tot}} = \sum m_i \mu_{mi}, \quad (2)$$

where  $m_i$  is the mass fraction contributed by the  $i$ th element having mass absorption coefficient  $\mu_{mi}$ .

With wavelengths of the order of 0.1 nm, the electromagnetic field of the photon interacts almost exclusively with the atomic electrons. Three different interactions contribute to the absorption process: true (photoelectric) absorption, Compton scattering, and Rayleigh scattering. All three phenomena are, at least to a small degree, dependent upon the chemical binding of the component atoms [5]. As a consequence, x-ray transmission measurements usually will not yield a precise determination of sample density if the calculation is based on a value for  $\mu_m$  determined via Eq. (2). In fact, there is a difference of approximately 5% between the previously measured value of  $\mu_m$  for carbon dioxide [6] and the calculated value based on Eq. (2). This problem is not central to the study of critical phenomena since the relevant density is a reduced quantity based on the critical density. The crucial consideration for this work is whether or not  $\mu_m$  remains constant as the sample approaches the critical point. The only one of the three interactions which could have a noticeable change is the Rayleigh scattering component. The Rayleigh component probably contributes about 2.5% of the total absorption coefficient for carbon dioxide for x rays with a wavelength of 0.154 nm [7]. For a sample near the critical

point, Rayleigh scattering gives rise to critical opalescence, which for x rays is limited to the small-angle region [8].

Simple calculations were performed to estimate the contribution to the Rayleigh cross section expected from critical scattering. (See the Appendix.) The calculations indicate that critical scattering will change  $\mu_m$  by approximately 0.01% for the conditions of this study, over the temperature region where  $t < 10^{-3}$ . This should be a negligible change for the purposes of this work.

The major advantage of this x-ray absorption method would seem to be that the experimental method is fundamentally different from the optical or capacitive methods and hence the determination of the density of the phases is based on quite different considerations. One of the disadvantages associated with the x-ray method is introduced due to the counting statistics. The accuracy of the data is related to number of counts  $N$  that the detector collects in a given time through the square root of  $N$ . In other words, to increase the accuracy of the results by a factor of 2, the number of counts would need to be quadrupled. For practical reasons, it may be difficult to exceed about  $10^7$  total counts for our experiments. Another concern that must be overcome is the change in x-ray beam intensity due to variations in the output of the power supply. These fluctuations will introduce variances in the transmissions and thus also in the densities, though the slopes of the profiles will remain unchanged. The effect of the variation in the power supply can be minimized by collecting several sets of reference and sample intensities (20 sets for our experiments), each set being collected over a period of approximately 1 min. This x-ray technique is similar to a radioactive tracer method used earlier by Weinberger and Schneider [9,10]. Previously, Schmidt and co-workers used an x-ray transmission method employing a special slit scanning system to obtain density profiles of argon in the critical region [11].

### III. EXPERIMENTAL PROCEDURE

#### A. The sample cell

The sample cell body was machined from 4-in.-diam cylindrical copper stock, 4 in. in length. For transmission measurements, it is necessary to accurately measure the x-ray beam intensity with both the sample cell and a reference cell in the beam. To accommodate these measurements, two compartments were machined into the central region of the cell block. The compartments were 1.0 cm in height, 0.50 cm in width, and 0.48 cm thick and were positioned equidistantly from the cylindrical axis of the cell. The cell block could be rotated about the vertical axis so that both sample cell and reference cell could be conveniently positioned in and out of the x-ray beam. Two flanges, together with beryllium disks and indium gaskets, were used to seal the two chambers. The sample block was symmetrically positioned inside a vacuum chamber. All surfaces of the cell and the chamber were given a high polish and a radiation shield surrounded the cell.

The top 2.0 cm of the cell was machined down to a 2.5

cm diameter to provide a neck on which the cell heaters were wound. Two heaters were fixed to the cell: a constant current heater from the power supply and a heater controlled by the temperature control circuit.

Three lines were drilled through the neck and side of the cell in order to access the sample compartment for filling with carbon dioxide. Once the through lines for the fill system and the valve were connected, the drill points in the cell body were soldered closed to complete the seal in the cell portion of the fill line. The sample compartment could be opened or closed via a Whitey Type B-OKM2 valve. The body of the valve was machined down to an approximate 1.3 cm diameter and inserted into the body of the copper cell lateral to the carbon dioxide compartment. The shaft of the valve was cut down to a hex-head for use with a retractable feedthrough from the outside of the vacuum chamber in order that the sample compartment could be opened or closed repeatedly without removing the cell from the vacuum chamber. Please refer to Fig. 1 for a cross section of the sample cell.

The sample cell was suspended from the neck by a 1.0-cm-diam steel rod 10 cm long. An O-ring between the rod and vacuum chamber cover provided a dynamic vacuum seal for the chamber. Above the cover, the rod was attached concentrically to a 5-cm-diam, 8-cm-long solid aluminum cylinder. The bottom of the aluminum cylinder rested on the chamber cover via a roller thrust bearing which made possible the free rotation of the cylinder-and-sample cell system in order to position the sample cell in the proper orientation for the two measurements necessary for the x-ray transmission calculation. The steel rod also served as the "heat leak" for the sample cell. The atmosphere surrounding the aluminum cylinder was the cold reservoir for the system at a tem-

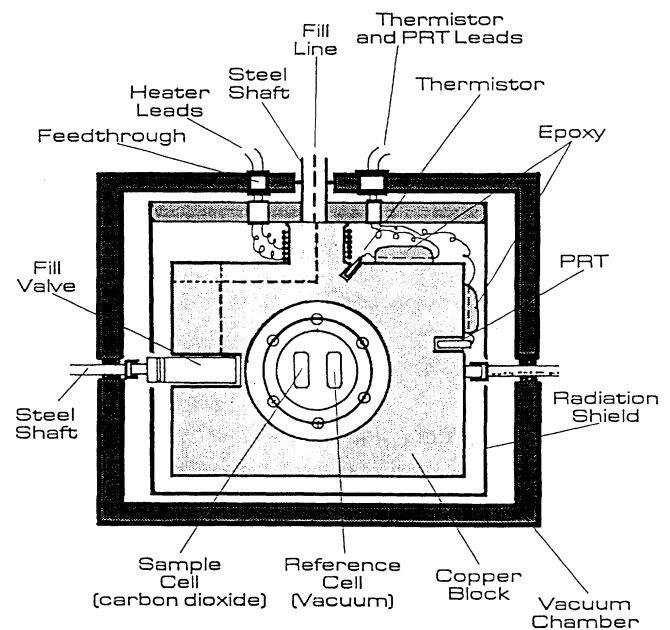


FIG. 1. Sample cell for x-ray transmission measurements. The platinum resistance thermometer is designated as PRT.

perature of  $22 \pm 1^\circ\text{C}$ . The steel rod had a 3-mm hole drilled along its axis to provide access for the 0.063-in. stainless steel fill line to the gas inlet at the neck of the sample cell. The carbon dioxide used for the study was research grade, 99.995% purity, purchased from Matheson Gas Products Co.

### B. X-ray collimation and detection system

The x-ray source was a standard Philips fixed copper target x-ray tube energized by a Westinghouse high voltage supply. The tube high voltage was limited to 16 kV to avoid the generation of x rays having energies twice that of the Cu  $K\alpha$  radiation. The power output of the supply was regulated so that, after a warm-up period, the x-ray intensity remained constant within approximately 1%. This stability was not nearly adequate for the required transmission measurements and consequently a repetitive measurement procedure was used in order to reduce the effect of the x-ray beam intensity drift by an order of magnitude.

After passing through a 1.0-mm collimation tube, the x rays impinged on a UCAR (Union Carbide) Grade ZYA graphite monochromator adjusted to reflect the Cu  $K\alpha$  characteristic wavelength. The mosaic spread for the crystal of  $0.4^\circ$  insured that the monochromatic reflected radiation had a beam divergence of about  $0.4^\circ$ . The evacuated diverging beam path had a total length of 164 cm. The sample under study was mounted midway between the monochromator and the x-ray detector.

A one-dimensional position sensitive detector was mounted with its axis oriented vertically so that the x-ray intensity profile of the transmitted diverging beam could be monitored accurately. The detector used was a 5-cm gas-filled flow through proportional counter, of the "backgammon" design made by the M. Braun Company. The resolution of the detector for Cu  $K\alpha$  radiation was approximately  $150 \mu\text{m}$ . Because of the diverging beam geometry, the resolution at the sample was near  $100 \mu\text{m}$ . The maximum counting rate for the detector was slightly under  $10^4$  counts/s.

The data output of the detector was stored with a multichannel analyzer (MCA). For our application, the MCA was programmed to divide the 8192 channels into eight separate banks of 1024 channels, though only two of the banks were actually used to store the transmission data. A microprocessor controller routed the detector data to the first two banks of the MCA. The first bank collected the x-ray intensity data from the carbon dioxide sample, while the second bank collected the data for the reference intensity.

The detector and the MCA each had dead times of  $10^{-5}$  s. The combination had a measured dead time of  $1.22 \times 10^{-5}$  s. Each channel of the detector represents an increment of the height in the sample cell of  $2.742 \times 10^{-3}$  cm. The diverging x-ray beam reaching the detector had roughly a Gaussian intensity profile in the vertical direction with a full width at half maximum intensity of approximately 200 channels, which examined a region near the middle of the sample of approximately 5.5 mm in height. The cutoff intensity for data analysis purposes

was taken to be about 7000 counts per channel. This meant that of the 300 MCA channels which collected data for the density profile, roughly the middle 220–230 channels were used for the actual data analysis.

### C. Error analysis

There are two primary sources of error in the x-ray transmission measurements. One is the error associated with the counting statistics and the other is due to the instability of the incident beam intensity. Both of these effects contribute to the experimental uncertainty in the determination of the density of the fluid.

The relation of the density of the phase to the two intensity measurements and the transmission  $T_x$  is of the form

$$\rho = -\frac{1}{\mu_m x} (\ln I - \ln I_0) = -\frac{\ln T_x}{\mu_m x}. \quad (3)$$

Under the experimental conditions used in this study, the statistical error can be reduced by covering the reference window with nickel foil. This has the effect of attenuating the incident beam so it is on the order of the transmitted beam. The measured reference intensity with the foil in place  $I'_0$  is then related to the reference intensity without the foil  $I_0$  by the equation

$$I_0 = FI'_0, \quad (4)$$

where  $F$  is a constant factor for the nickel foil. With the foil in place, the density equation (3) becomes

$$\rho = -\frac{1}{\mu_m x} (\ln I - \ln I'_0 - \ln F). \quad (5)$$

If  $\Delta\rho$  is the change in the density  $\rho$  due to random changes in  $I$  and  $I'_0$ , then an error equation can be written, having the form

$$\Delta\rho = \frac{1}{\mu_m x} \left[ \left( \frac{\partial \ln I}{\partial I} \Delta I \right)^2 + \left( \frac{\partial \ln I'_0}{\partial I'_0} \Delta I'_0 \right)^2 \right]^{1/2} \quad (6)$$

or

$$\Delta\rho = \frac{1}{\mu_m x} \left[ \left( \frac{\Delta I}{I} \right)^2 + \left( \frac{\Delta I'_0}{I'_0} \right)^2 \right]^{1/2}, \quad (7)$$

where  $\Delta I$  and  $\Delta I'_0$  are the respective fluctuations in the measurement of the transmitted and the modified reference x-ray beam intensities. The standard deviation  $\sigma$  for the density determination will be equal to the uncertainty in the density measurement  $\Delta\rho$  if

$$\Delta I = \frac{\sqrt{I\tau}}{\tau}, \quad \Delta I'_0 = \frac{\sqrt{I'_0\tau}}{\tau}, \quad (8)$$

where  $\tau$  is the counting time. Then, the standard deviation is given by

$$\sigma = \frac{1}{\mu_m x} \left[ \frac{1}{I\tau} + \frac{1}{I'_0\tau} \right]^{1/2} \quad (9)$$

and the fractional deviation in the density  $\delta$  is given by

$$\delta = \frac{\sigma}{\rho} = -\frac{1}{\ln T_x} \left( \frac{1}{I\tau} + \frac{1}{I'_0\tau} \right)^{1/2}. \quad (10)$$

This equation can be rewritten in terms of the transmission and the constant factor  $F$  yielding

$$\delta = -\frac{1}{\sqrt{I'_0\tau \ln T_x}} \left( \frac{1}{FT_x} + 1 \right)^{1/2}. \quad (11)$$

$I'_0$  should be adjusted to be close to the maximum acceptable counting rate for the detector. In this experiment, that rate is about  $10^4$  counts/s. From Eq. (11), it appears that  $\delta$  can be reduced by making  $F$  large; however, if  $FT_x > 1$ , then  $I$  will be greater than the previously set value for  $I'_0$  and will exceed the maximum counting rate for the detector. From these considerations, it can be seen that the thickness of the nickel foil should be chosen such that the product  $FT_x$  is approximately equal to 1 for the vapor phase, since it has the highest transmission. The foil used for the experiment had a value for  $F$  of about 5 and consisted of four thicknesses of 0.001-cm x-ray filter quality nickel foil. Typical experimental values of  $T_x = 0.15$  and  $I'_0\tau = 2 \times 10^4$  counts/channel will yield  $\delta = 0.0057 = 0.57\%$  for the standard deviation for a density determination based on the counts accumulated in one channel of the MCA. The expected standard deviation for the mean density, typically averaged over 100 channels, is  $\delta = 0.057\%$ . The expected error for the calculated density of the phase (either vapor or liquid) at the interface will depend upon the curve fitting method used in the analysis. Based on the above considerations, the error in our determination of the density of either phase at the vapor-liquid interface due to counting statistics was assumed to be about 0.13%.

Errors due to the instability of the x-ray beam intensity are primarily due to the changes in the input line voltage of the x-ray tube's power supply. These variations in the supply voltage were reduced to approximately 1% through the use of a Sorenson ac line voltage stabilizer and an electron beam current regulator for the x-ray tube. In addition, the x-ray source remained energized during the entire time during which the data were collected in order to avoid transients which would occur during the warm-up period. A change of beam intensity  $\Delta I_0$  will result in a change in the corresponding density  $\Delta\rho$ , given by

$$\Delta\rho = \frac{1}{\mu_m x} \left( \frac{\Delta I_0}{I_0} \right). \quad (12)$$

The fractional change in density will be given by

$$\frac{\Delta\rho}{\rho} = -\frac{1}{\ln T_x} \left( \frac{\Delta I_0}{I_0} \right). \quad (13)$$

For typical values of  $(\Delta I_0/I_0) = 0.01$  and  $T_x = 0.15$ , the fractional change in the density is about 0.53%. If 20 pairs of measurements of  $I_0$  and  $I$  are made, the error in the density calculation due to drift of the x-ray beam intensity should be less than 0.10%. These considerations indicate that the experimental uncertainty for the density

determination of either phase at the vapor-liquid interface should usually be less than 0.17%.

## IV. RESULTS AND DISCUSSION

### A. Density profiles

This study involved the collection of data on two separate fillings of the sample cell with carbon dioxide. For the first sample, data were collected for 26 density profiles at controller temperatures ranging from nearly  $10.5^\circ\text{C}$  below the critical temperature  $T_c$  to about  $3.3^\circ\text{C}$  above  $T_c$ . The temperature of the sample was set to a certain value and then the cell was allowed to come to equilibrium over a 4-h period before the x-ray transmission data were accumulated. Once the data were collected for a specific temperature setting, the temperature was changed and the process was repeated for the next density profile. The minimum change in the temperature control setting between measurements for the first sample was approximately  $0.02^\circ\text{C}$ .

For the second sample, data were collected for 65 density profiles at temperatures ranging from about  $8.7^\circ\text{C}$  below  $T_c$  to about  $2.1^\circ\text{C}$  above  $T_c$ . Special attention was given to the temperature region very close to  $T_c$  where the temperature interval between successive measurements was reduced to  $0.002^\circ\text{C}$ . The time for the sample to equilibrate following a change in temperature was increased to 6 h. This increase in time seemed advisable since the time required for the system to reach equilibrium is expected to increase for temperatures near  $T_c$  [12].

Typical density profiles are illustrated in Figs. 2–4. Error ranges corresponding to plus or minus one standard deviation are included on each graph. Density profiles at temperatures below  $T_c$  have an error range for each fluid phase, while profiles above  $T_c$  have a single error range, since only one phase is present. The error ranges are relevant to the expected error near the middle of the profile, with errors being larger at the ends. In Fig. 2, the liquid-vapor transition appears to take place over a distance corresponding to four or five detector channels, or roughly  $120\ \mu\text{m}$ . This is consistent with what would be expected for a sharp phase separation observed with a

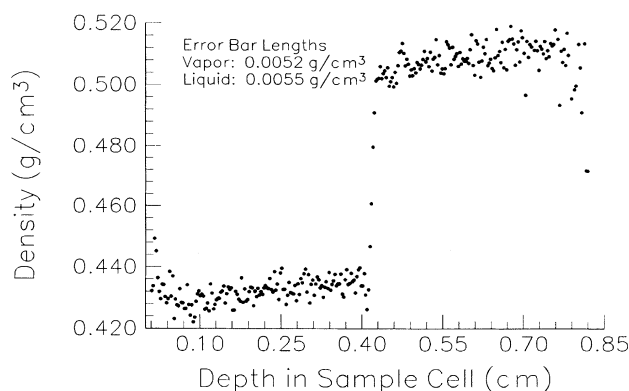


FIG. 2. Density profile for carbon dioxide for sample 2,  $0.0200^\circ\text{C}$  below  $T_c$ .

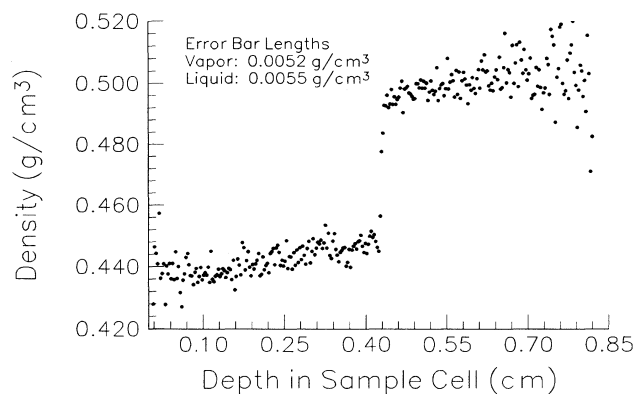


FIG. 3. Density profile for carbon dioxide for sample 2, 0.0020 °C below  $T_c$ .

detector having a resolution of 100  $\mu\text{m}$ .

Figures 3 and 4 both show positive slopes for the graphs which are related to the high compressibility of the fluid near the critical point. It can be seen that a visual examination of the density profiles will not readily yield the point at which the critical point occurs. Both Fig. 3, in which the sample is below the critical point, and Fig. 4, in which the sample is above the critical point and in the one-phase region, exhibit similar features of very steep slopes of the density profile as well as a rounding of the profile in the transition region. Appropriate curve fitting techniques were used with the density profiles to determine the densities of the coexisting phases. The densities of the coexisting phases are listed in Tables I and II.

#### B. Determination of the critical temperature

The density data were used to determine the critical temperature for each sample. Specifically, since our temperature monitor was not calibrated, only the monitor reading corresponding to the critical temperature could be determined. The usual method of analysis [13,14] makes use of the scaling law for the order parameter or the law with corrections to scaling. The latter was writ-

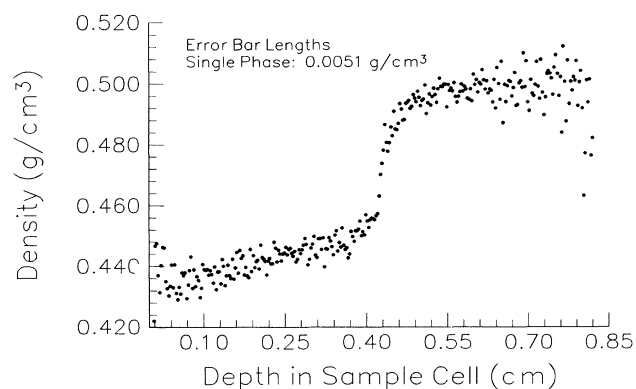


FIG. 4. Density profile for carbon dioxide for sample 2, 0.0050 °C above  $T_c$ .

TABLE I. Density data for CO<sub>2</sub> sample 1.

$T - T_c$ (°C)	Density (g/cm <sup>3</sup> )	
	Vapor	Liquid
-10.304	0.2100	0.7616
-6.827	0.2407	0.7219
-3.832	0.2790	0.6745
-1.812	0.3192	0.6239
-0.829	0.3517	0.5872
-0.541	0.3674	0.5678
-0.327	0.3831	0.5534
-0.217	0.3930	0.5423
-0.167	0.3996	0.5362
-0.120	0.4063	0.5294
-0.091	0.4123	0.5228
-0.074	0.4143	0.5182
-0.041	0.4242	0.5075
-0.017	0.4364	0.5007
-0.016	0.4310	0.5010

TABLE II. Density data for CO<sub>2</sub> sample 2.

$T - T_c$ (°C)	Density (g/cm <sup>3</sup> )	
	Vapor	Liquid
-8.718	0.2274	0.7472
-8.394	0.2292	0.7458
-6.886	0.2450	0.7234
-6.884	0.2438	0.7218
-5.424	0.2621	0.7021
-3.840	0.2833	0.6737
-1.852	0.3258	0.6260
-0.852	0.3609	0.5880
-0.788	0.3611	0.5852
-0.552	0.3744	0.5732
-0.346	0.3886	0.5565
-0.344	0.3890	0.5539
-0.244	0.3975	0.5470
-0.182	0.4032	0.5390
-0.158	0.4064	0.5331
-0.154	0.4071	0.5346
-0.146	0.4086	0.5315
-0.106	0.4147	0.5263
-0.066	0.4234	0.5176
-0.052	0.4265	0.5121
-0.026	0.4344	0.5050
-0.022	0.4365	0.5030
-0.020	0.4404	0.4996
-0.018	0.4407	0.4982
-0.012	0.4414	0.4974
-0.011	0.4461	0.4926
-0.010	0.4455	0.4939
-0.009	0.4460	0.4921
-0.007	0.4496	0.4907
-0.006	0.4507	0.4885
-0.002	0.4503	0.4819

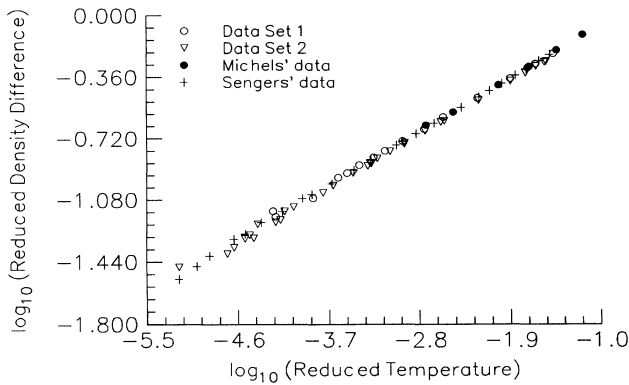


FIG. 5.  $\log_{10}$  (reduced density difference) vs  $\log_{10}$  (reduced temperature) for the data of Michel, Blaisse, and Michel, the data of Levelt-Sengers, Straub, and Vicentini-Missoni, and data sets 1 and 2.

ten for the actual fitting procedure as

$$\frac{\rho_l - \rho_v}{2\rho_c} = \Delta\rho = B_0 \left[ \frac{T_c - T}{T_{c0}} \right]^\beta + B_1 \left[ \frac{T_c - T}{T_{c0}} \right]^{\beta+\Delta} + B_2 \left[ \frac{T_c - T}{T_{c0}} \right]^{\beta+2\Delta}, \quad (14)$$

where  $T$  is the reading from the temperature monitor,  $T_c$  is the critical temperature parameter, measured with respect to the monitor, and  $T_{c0} = 304.2$  K is the literature value for the critical temperature of carbon dioxide. Figure 5 illustrates the power law behavior of the reduced density difference of the phases versus reduced temperature for both data sets. By way of comparison, Fig. 5 also shows the data for carbon dioxide collected by Michels, Blaisse, and Michels [15] and Levelt-Sengers, Straub, and Vicentini-Missoni [1]. All four curves show a near linear behavior on the log-log graph as predicted by the scaling law. The data from both samples in this study are in excellent agreement with each other and also with the data

of Michels, Blaisse, and Michels and Levelt-Sengers, Straub, and Vicentini-Missoni.

For the temperature determination, the Ising model predicts a value for  $\beta$  to be about 0.327. The value of  $\Delta$  was fixed at 0.5. The fitting procedure that was used involved a series of trials in which  $T_c$  was incremented and the parameters  $\beta$ ,  $B_0$ ,  $B_1$ , and  $B_2$  in Eq. (14) were either fixed or allowed to vary in order to achieve a fit for each value of  $T_c$ . For a given set of model conditions, the value chosen for  $T_c$  was the value which gave the smallest mean square residual for the fit. Results of these calculations, summarizing the fitted parameters of  $\beta$ ,  $B_0$ ,  $B_1$ , and  $B_2$  for the scaling law, are presented in Table III. The results presented were found in conjunction with the calculated critical densities, which will be discussed next. The preferred method of determining  $T_c$  is the one which makes use of the Ising model value for  $\beta = 0.327$ . The values of  $B_0$  and  $B_1$  obtained for the fits to both samples are consistent with Moldover's study [16]. For  $\text{CO}_2$ , his values for  $B_0$  were 1.59 and 1.60, based on two different approaches. Studies on other systems suggest that  $B_1$  should be positive and have magnitude about the same as  $B_0$ . This comparison is encouraging; however, when  $\beta$  is allowed to vary, the fit using corrections to scaling resulted in slightly lower mean square residual (MSR) values, but the  $\beta$  and  $B_1$  values are no longer acceptable, i.e.,  $\beta$  no longer matches the Ising model value and  $B_1$  was negative. This failure would seem to indicate that the data were not completely free of some type of systematic error. Results for fitted straight lines for both samples are summarized in Table III. The MSR values for this fit with sample 1 were only about one-half the MSR values of sample 2. The difference, which is evident from Fig. 5, is a result of the fact that sample 1 had only three measurements in the temperature range  $t < 2 \times 10^{-4}$ , while sample 2 had twelve measurements in this region. The temperature measurement and control stability of about  $\pm 0.001$  °C becomes progressively more of a limitation as the system moves into the  $t < 10^{-4}$  region.

The monitor values determined for  $T_c$  for the two sam-

TABLE III. Results of fitting process to determine the monitor reading corresponding to  $T_c$  using the scaling law.  $R$  is the mean square residual.

Sample	$\beta$	$B_0$	$B_1$	$B_2$	$T_c$ (monitor reading)	$10^5 R$
1	0.3409	1.8898			2.3278	0.5923
1	0.3452	1.9497	-0.1866		2.3286	0.5160
1	0.3411	1.8833	0.2237	-1.0731	2.3282	0.5143
1	0.3270 (fixed)	1.6765	1.3835	-3.8928	2.3267	0.5313
2	0.3446	1.8453			2.3500	1.0340
2	0.3520	1.9542	-0.3790		2.3504	0.9882
2	0.3539	1.9888	-0.6410	0.8244	2.3504	0.9874
2	0.3270 (fixed)	1.5695	2.1014	-6.9448	2.3495	1.1227

TABLE IV. Determination of the critical density via the scaling law.

Sample	$T_c$ (monitor reading)	Critical density $\rho_c$ (g/cm <sup>3</sup> )	$\beta_v$	$\beta_l$	$B_{0v}$	$B_{0l}$
1	2.328	0.4635	0.3441	0.3419	1.7803	2.0126
2	2.350	0.4677	0.3466	0.3473	1.7753	1.9644

ples differ by 0.022 °C (about 0.007%). This difference in  $T_c$  probably reflects a slight difference in the impurities of the samples and/or the change in the characteristics of the temperature monitor system over a period of 3 months.

### C. Determination of the critical density

As with the determination of the critical temperature of samples, the fitting procedure for the critical densities made use of the scaling law. The model used was of the form

$$\Delta\rho_{\text{ph}} = \frac{|\rho_{\text{ph}} - \rho_c|}{\rho_c} = B_0 \left( \frac{T_c - T}{T_{c0}} \right)^\beta, \quad (15)$$

where  $\rho_{\text{ph}}$  is the density of the liquid or vapor phase and  $\rho_c$  is the critical density estimate. Other variables in Eq. (15) are the same as those used in Eq. (14).

A series of log-log plots of  $\Delta\rho_{\text{ph}}$  for each phase versus the reduced temperature were made for various estimates of the critical density. Since both vapor and liquid phases belong to the same universality class, the value of the critical density was varied until the  $\beta$  value for each phase was approximately the same. Ideally, the method should be applied to data for  $t < 10^{-3}$  where the scaling law should be more closely observed than over the extended temperature range used here. However, the limitation of the data for sample 1 at very small reduced temperatures was the reason for using the analysis followed here. In addition to the critical exponent  $\beta$ , values for the leading term in the scaling law  $B_0$  were also obtained for each phase. Results of the analysis, presented in Table IV, are based on the mass absorption coefficient determined by Stockmeyer [6]. The calculated values for the critical density for sample 2 is in close agreement with the accepted value for CO<sub>2</sub>, 0.468 g/cm<sup>3</sup>.

### D. Rectilinear diameter

For most nonconducting fluids, the 100-yr-old empirical law of the rectilinear diameter  $\rho_d = (\rho_l + \rho_v)/2\rho_c$  has been found to hold surprisingly well over an extended temperature range. However, modern theories predict that the reduced temperature derivative of the rectilinear diameter  $d\rho_d/dt$  should diverge as  $t$  approaches zero at least as fast as the constant volume specific heat  $c_v$  [13,17]. That is,  $\rho_d$  should vary as

$$\rho_d = 1 + A_{1-\alpha}t^{1-\alpha} + A_1t + A_2t^2 + \dots \quad (16)$$

Since  $1-\alpha=0.89$  is very close to unity, the true singularity is difficult to separate from the linear temperature term.

Studies on carbon dioxide by Levelt-Sengers, Straub, and Vicentini-Missoni [1] have indicated that the law of rectilinear diameters hold to temperatures within 0.002°C of the critical point, showing no divergence from linearity. The data collected during both trials in this study indicated that there may be reason to doubt this conclusion. Figure 6 shows the plot of the coexistence curve diameter  $\rho_d$  versus reduced temperature for both of the samples investigated in this study. It is evident in both curves that there is a marked divergence from the linear behavior predicted by the law of rectilinear diameter as the sample temperature approaches the critical point. Equation (16) shows that with the sample temperature well below  $T_c$ , the linear term in the equation will dominate. This term is responsible for the established linear behavior of the rectilinear diameter in the region  $t > 10^{-3}$ . Figure 7 is a graph of the coexistence curve diameter for measurements made in the range  $t > 6 \times 10^{-4}$ . The data are fitted to the equation

$$\rho_d = A_0 + A_1t. \quad (17)$$

$A_0$  would, of course, be unity if the equation were exact. The outer reduced temperature regions of both data sets were used to calculate a fit based on Eq. (17). The fitted values of  $A_0$  for samples 1 and 2 were  $1.0091 \pm 0.0024$  and  $1.0089 \pm 0.0017$ , respectively. These values for the coefficient  $A_0$  were compared to values of  $A_0$  obtained by directly averaging the interior points of both data sets. For sample 2, there were ten density measurements collected at reduced temperatures, in the range  $10^{-4} > t > 10^{-5}$ . The mean value for these average densities was  $1.0041 \pm 0.0007$ . This means that an anomaly of approximately 0.5% in the rectilinear diameter is indicated. For sample 1, the evidence is less convincing as there

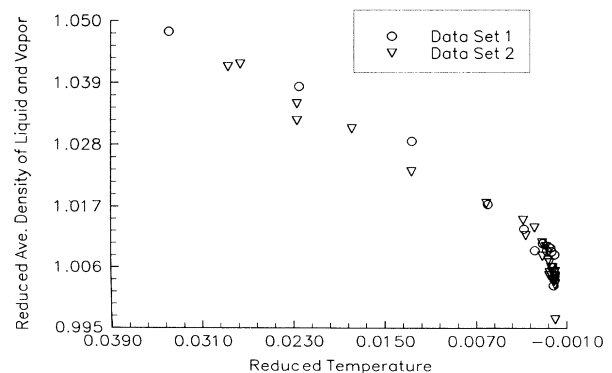


FIG. 6. Rectilinear diameter of carbon dioxide for data sets 1 and 2.

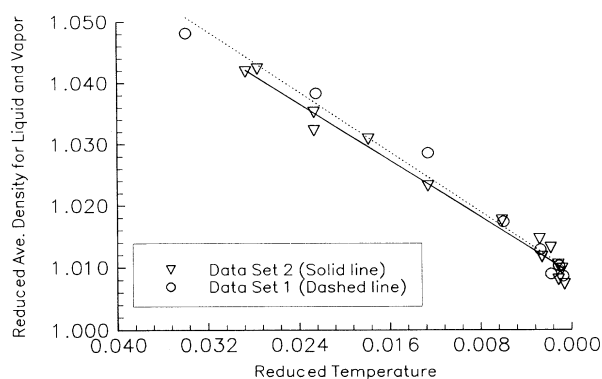


FIG. 7. Rectilinear diameter of carbon dioxide for data sets 1 and 2, outer points.

were only three density measurements made in the same temperature interval, with a mean of  $1.0048 \pm 0.0024$ , approximately 0.4% below the value for  $A_0$  based on a linear extrapolation. These estimates of the deviation from linear behavior indicate the anomaly in  $\text{CO}_2$  is relatively large compared to the five fluids studied by Pestak *et al.* [3], although few of these measurements were at  $t < 10^{-4}$ . For  $\text{SF}_6$ , the anomaly is about 0.25%, which is the largest of the group. They believe the magnitude of the singularity arises due to the contribution of three-body forces to the interaction potential, which can be estimated by the product of the molecular polarizability and the critical particle density. On the other hand, Singh and Pitzer [19] questioned whether the relative strength of the three-body forces is the key characteristic that determines the extent of the singularity. They proposed that the magnitude of the anomaly is more closely related to an acentric factor, which is a measure of the deviation of the pair potential from spherical symmetry. According to this theory,  $\text{CO}_2$  should have a larger singularity than that of  $\text{SF}_6$ , although the acentric factor for  $\text{CO}_2$  is only 7.5% larger than that for  $\text{SF}_6$ .

#### E. Estimates for the isothermal compressibilities

The study of the isothermal compressibility for the coexisting phases was of special interest to this investigation because theoretical analyses predict that the compressibility should have a discontinuity across the coexistence curve [3]. The dimensionless compressibility  $K'_T$  is related to the reduced temperature through a simple scaling law of the form

$$K'_T = P_c K_T = \Gamma' t^{-\gamma'} \quad (18)$$

where  $\gamma' = 1.26$  from the Ising model calculations and  $P_c = 7.38 \times 10^7 \text{ dyn/cm}^2$  is the critical pressure for carbon dioxide. Primed quantities are for temperatures below the critical point, while unprimed quantities are above the critical point. Other studies on  $\text{CO}_2$  [18] have estimated  $\Gamma'$  to be approximately  $1.19 \times 10^{-2}$ . If the compressibility does have a discontinuity across the coexistence curve as the reduced temperature approaches zero, then  $\Gamma'$  will likewise have different values for the

two phases. The slope of the coexistence curve  $m$  can be written as

$$m \equiv \frac{\partial \rho}{\partial z} = g \rho^2 K_T = \frac{1}{P_c} (g \rho^2 \Gamma' t^{-\gamma'}) \quad (19)$$

Attempts to calculate  $K_T$  for nine of the density profiles having the smallest reduced temperatures were inadequate to establish any singularity in  $K_T$  for the coexisting phases. This failure is primarily a direct consequence of the uncertainty imposed on the calculation by the counting statistics.

The value of  $\Gamma$  corresponding to the critical isochore of the single phase region is nearly five times larger than  $\Gamma'$  for the coexisting phases [20]. As a consequence, the density profiles above  $T_c$  exhibit larger slopes of the density profile than observed at the corresponding reduced temperature profiles below  $T_c$ . This distinction is evident upon comparison of Figs. 3 and 4.

## V. SUMMARY AND CONCLUSIONS

### A. The carbon dioxide study

The density profiles for carbon dioxide obtained via the x-ray absorption method were similar to those obtained by optical techniques and demonstrated the expected characteristics in the critical region. The majority of the experiments and analyses were concerned with the study of the coexistence region. These analyses indicate the following.

(i) The behavior of the reduced densities for both samples in the study is in close agreement with the best available optical data.

(ii) A theoretically predicted singularity in the rectilinear diameter at temperatures close to  $T_c$  was observed for both samples. The singularity, which had not been observed in a previous analysis of optical data, appeared to have a larger magnitude than that which has been observed in other nonconducting fluids.

(iii) Statistical error and resolution limitations of the detector prevented the determination of the density profiles with sufficient accuracy to confirm the predicted discontinuity of the isothermal compressibility across the coexistence curve.

### B. X-ray absorption technique

The x-ray absorption technique affords a fairly convenient and reliable method of determining the density profile of both transparent and opaque fluids which are in the critical region. There are few underlying theoretical concerns about the experiment other than the consistency of the mass absorption coefficient of the material over the critical region. Theoretical arguments presented indicate that for reduced temperatures below  $t^{-3}$  the absorption coefficient should remain constant within 0.01%.

The two primary experimental errors associated with the technique are the uncertainty introduced by counting statistics and the error due to the instability of the x-ray beam. Current improvements in position sensitive detector technology will permit the use of much higher x-ray

or  $\gamma$ -ray beam intensities, which makes the future application of the absorption experiment very attractive.

#### APPENDIX: CRITICAL SCATTERING

Critical x-ray scattering, which is a direct consequence of the divergence of the long-range correlation length, makes its contribution to the scattering pattern over the small-angle region. For our consideration here, the phenomenon is adequately represented by the Ornstein-Zernike (OZ) approximation [21]

$$dI_{OZ}(q) = \frac{I_i I_e \rho_e^2 A k_B T K_T dx}{y^2 (1 + q^2 L^2)}, \quad (\text{A1})$$

where  $dI_{OZ}(q)$  is the intensity scattered by the thickness  $dx$ .  $I_i$  is the incident x-ray beam intensity at the increment  $dx$ ,  $I_e$  is the electron scattering cross section,  $\rho_e$  is the electron density of the sample,  $A$  is the cross section of the irradiated sample,  $k_B$  is the Boltzmann constant,  $T$  is the absolute temperature,  $K_T$  is the isothermal compressibility,  $L$  is the long-range correlation length, and  $y$  is the sample-to-detector distance. The magnitude of the momentum transfer vector is

$$q = \frac{4\pi \sin \left[ \frac{\theta}{2} \right]}{\lambda}, \quad (\text{A2})$$

where  $\theta$  is the scattering angle and  $\lambda$  is the x-ray wavelength. Both  $K_T$  and  $L$  diverge as the reduced temperature approaches zero,

$$K_T \sim t^{-\gamma} \quad (\text{A3a})$$

and

$$L \sim t^{-\nu}, \quad (\text{A3b})$$

but since  $\nu = \gamma/2$ ,

$$\frac{K_T}{L^2} = C, \quad (\text{A3c})$$

where  $C$  is a constant. The scattering curve described by Eq. (A1) has three distinct regions: (i) the inner region, where

$$I(q) \approx I(0) \sim K_T, \quad q^2 L^2 \ll 1;$$

(ii) the outer region, where

$$I(q) \sim \left[ \frac{K_T}{L^2} \right] \frac{\rho_e^2 T}{q^2}, \quad q^2 L^2 \gg 1;$$

and (iii) the transmission region, between regions 1 and 2, where

$$0.1 < q^2 L^2 < 10.$$

#### 1. Effect of the critical scattering on the detector resolution

For the diverging beam geometry used in this study, the active part of the position sensitive detector has a sufficiently large cross section ( $\sim 1 \text{ cm}^2$ ) that for  $t < 10^{-3}$ ,

nearly all of the inner region of the scattering pattern will be captured by the detector. This portion of the scattering contributes to the measured transmitted beam and consequently it will not affect the average transmission of the sample. Likewise, this scattered radiation captured by the detector does not effectively contribute to the Rayleigh scattering cross section. However, this scattering will lead to a "background term" for the density profile resulting from a net transfer of scattered photons between positions in the detector.

The background term can be readily estimated by calculating the total scattering power captured by the detector  $P_D = \int I_{OZ}(q) T_x d\Omega$ , where the integration is over the solid angle subtended by the detector and  $T_x$  is the transmission through the sample. We will assume a simplified geometry for which each unit of the sample is located along the perpendicular axis of a detector having a circular cross section of  $0.5 \text{ cm}^2$ . For a sample-to-detector distance  $y = 82 \text{ cm}$ , the maximum  $q$  value for scattered radiation captured by the detector will be  $q_0 = 0.20 \text{ nm}^{-1}$  and  $d\Omega = \lambda^2 q dq / 2\pi$ . For a sample of thickness  $x = 0.48 \text{ cm}$ , the fraction of the incident power reaching the detector due to critical scattering is given by

$$\frac{P_D}{I_0 A T_x} = I_e \rho_e^2 k_B T K_T \lambda^2 x \int_0^{q_0} \frac{q dq}{2\pi(1 + q^2 L^2)} \quad (\text{A4a})$$

or

$$\frac{P_D}{I_0 A T_x} = \frac{I_e \rho_e^2 k_B T K_T \lambda^2 x}{4\pi L^2} \ln(1 + q_0^2 L^2). \quad (\text{A4b})$$

Values for  $K_T$  and  $L$  were obtained from Lin's small-angle scattering measurements on carbon dioxide [22]. At  $t = 1.25 \times 10^{-3}$ , these measurements yield

$$\frac{K_T}{L^2} = 2.28 \times 10^6 \text{ dyn}^{-1}$$

and

$$L = 11.8 \text{ nm}.$$

Equation (A3b) was used to estimate  $L$  values for other reduced temperatures. Typical results are

$$\frac{P_D}{I_0 A T_x} \leq \begin{cases} 0.05\% & \text{for } t > 10^{-2} \\ 0.3\% & \text{for } t > 10^{-3} \\ 1.1\% & \text{for } t > 10^{-5}. \end{cases}$$

These results reflect the expected divergence of the critical scattering at very small angles. The quantity  $P_D / I_0 A T_x$  is probably not a true estimate of the error resulting from the presence of the scattering flux, since this ratio actually measures the radiation scattered from a given region on average. However, since radiation is scattered both into and out of a given region of the detector, the resulting error due to scattering, which is related to the net transfer, will certainly be considerably less than the values determined for the ratio  $P_D / I_0 A T_x$ .

## 2. Effect of the critical scattering on the Rayleigh scattering cross section

The portion of the critical scattering which occurs at sufficiently large angles such that it is not collected by the detector will decrease the sample transmission and effectively increase the Rayleigh scattering cross section. An estimate of the cross section due to critical scattering, represented by  $\sigma_{OZ}$ , can be made in terms of the same simplified geometry used in the preceding subsection. The intensity removed from the incident beam due to scattering from a mass increment  $dm$  will be given by

$$dI = I_0(\sigma_{OZ})dm ; \quad (A5a)$$

thus the cross section is given by

$$\sigma_{OZ} = \left[ \frac{1}{I_0} \right] \frac{dI}{dm} = \int_{q_0}^{q_{\max}} \frac{I_e \rho_e^2 k_B T K_T \lambda^2}{2\pi\rho(1+q^2L^2)} q dq . \quad (A5b)$$

The value  $q_{\max} = 2.65 \text{ nm}^{-1}$  was used for the purpose of the calculation. This choice was based on the observation that for the scattering patterns obtained from argon by Thomas and Schmidt [21], the critical scattering tended to merge with the large-angle pattern at approximately this location. This gives a cross section of

$$\sigma_{OZ} = \frac{I_e \rho_e^2 k_B T K_T \lambda^2}{4\pi\rho L^2} \ln(1+q^2L^2)_{q_0}^{q_{\max}} . \quad (A5c)$$

For comparison purposes, the calculated values for  $\sigma_{OZ}$  can be expressed as a percentage of the actual value of the mass absorption coefficient used in the data analysis, which is  $\mu_m = 9.15 \text{ cm}^2/\text{g}$ . Typical results for  $\sigma_{OZ}/\mu_m$  over the range of reduced temperatures used in this study are presented in Table V. It is clear from these results

TABLE V. Changes in Rayleigh cross section and errors in calculated densities due to critical scattering.

Reduced temperature $t$	$\sigma_{OZ}/\mu_m$ (%)	$\Delta\rho/\rho$ (%)
$3 \times 10^{-2}$	0.191	0.15
$10^{-2}$	0.263	0.08
$10^{-3}$	0.336	0.01
$10^{-4}$	0.343	0.001
$10^{-5}$	0.344	

that the effective Rayleigh cross section does not diverge as  $t$  approaches zero, but rather approaches a limiting value. In our calculations of the density profiles, we have assumed the mass absorption coefficient to be constant, independent of temperature. Since this is not actually the case, an error in the density calculations  $\Delta\rho/\rho$  will occur due to the change in  $\sigma_{OZ}$ . This error becomes

$$\frac{\Delta\rho}{\rho} = \frac{\Delta\sigma_{OZ}}{\mu_m} = \frac{\sigma_{OZ} - \sigma_0}{\mu_m} , \quad (A6)$$

where  $\sigma_0$  is the limiting value of  $\sigma_{OZ}$  as  $t$  approaches zero. The values of the error  $\Delta\rho/\rho$  are also included in Table V. The analysis shows that in the important temperature range  $t < 10^{-3}$ , the divergence of the critical scattering at very small angles should have a negligible effect on the density determination. As the reduced temperature increases beyond  $10^{-2}$ , errors in the calculated densities should become sufficiently large to be observable. Additional experiments in this temperature range above  $T_c$ , where density should be constant, would be helpful.

- [1] J. M. H. Levelt-Sengers, J. Straub, and M. Vicentini-Missoni, *J. Chem. Phys.* **54**, 5034 (1971).
- [2] M. W. Pestak and M. H. W. Chan, *Phys. Rev. Lett.* **46**, 943 (1981).
- [3] M. W. Pestak, R. E. Goldstein, M. H. W. Chan, J. R. deBruyn, D. A. Balzarini, and N. W. Ashcroft, *Phys. Rev. B* **36**, 599 (1987).
- [4] R. S. Shankland, *Atomic and Nuclear Physics*, 2nd ed. (McMillan, New York, 1960), pp. 199–213.
- [5] B. Koch and C. H. MacGillavry, in *International Tables for X-Ray Crystallography* (Kynoch, Birmingham, England, 1968), Vol. III, pp. 157–159.
- [6] W. Stockmeyer, *Ann. Phys. (Leipzig)* **12**, 71 (1932).
- [7] R. D. Evans, *The Atomic Nucleus* (McGraw-Hill, New York, 1955), p. 713.
- [8] A. S. Eisenstein and N. S. Gingrich, *Phys. Rev.* **62**, 261 (1942).
- [9] H. B. Palmer, Ph.D. thesis, University of Wisconsin, 1952.
- [10] M. A. Weinberger and W. G. Schneider, *Can. J. Chem.* **30**, 847 (1952).
- [11] P. W. Schmidt (private communication).
- [12] P. C. Hohenberg and B.I. Halperin, *Rev. Mod. Phys.* **49**, 435 (1977).
- [13] J. Weiner, K. H. Langley, and N. C. Ford, Jr., *Phys. Rev. Lett.* **32**, 879 (1974).
- [14] J. R. deBruyn and D. A. Balzarini, *Phys. Rev. A* **36**, 5677 (1987).
- [15] A. Michels, B. Blaisse, and C. Michels, *Proc. R. Soc. London Ser. A* **902**, 358 (1937).
- [16] M. R. Moldover, *Phys. Rev. A* **31**, 1022 (1985).
- [17] J. J. Rehr and N. D. Mermin, *Phys. Rev. A* **8**, 472 (1973).
- [18] M. Vicentini-Missoni, J. M. H. Levelt-Sengers, and M. S. Green, *J. Res. Natl. Bur. Stand. (U.S.)* **73A**, 563 (1969).
- [19] R. R. Singh and K. S. Pitzer, *J. Chem. Phys.* **92**, 3096 (1990).
- [20] M. R. Moldover, J. V. Sengers, R. W. Gammon, and R. J. Hocken, *Rev. Mod. Phys.* **51**, 79 (1979).
- [21] J. E. Thomas and P. W. Schmidt, *J. Chem. Phys.* **39**, 2506 (1963).
- [22] J. S. Lin, Ph.D. thesis, University of Kansas, 1970.

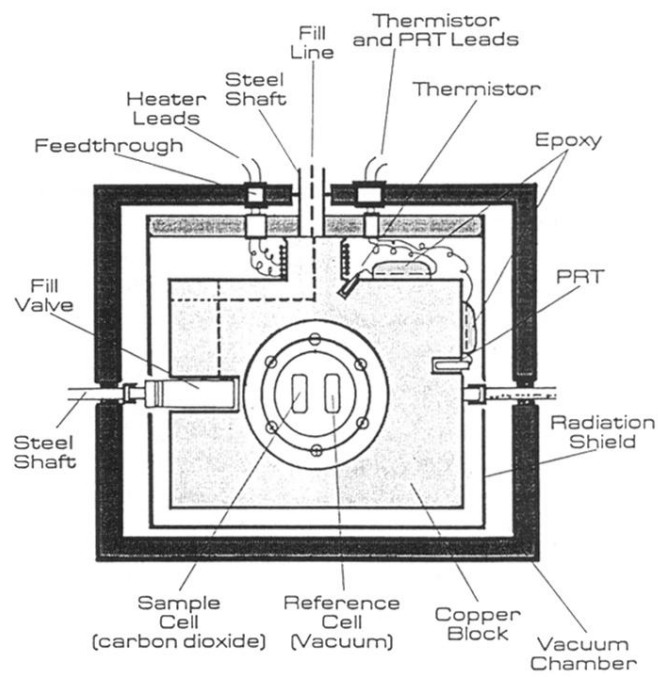


FIG. 1. Sample cell for x-ray transmission measurements. The platinum resistance thermometer is designated as PRT.